Integrated *in silico-in vitro* characterization, identification and disruption of the intermolecular interaction between SH3 domain-containing protein kinases and human pituitary tumor-transforming gene 1

Yanan Li[1],[*], Mengmeng Li[2],[*], Weijie Min[1], Guosheng Han[1], Laixing Wang[1], Chao Chen[1], Zifu Li[1], Yuhui Zhang[1], Jianmin Liu[1] and Zhijian Yue[1]

[1] *Department of Neurosurgery, Changhai Hospital, Second Military Medical University, Shanghai 200433, China*
[2] *Department of Rheumatology and Immunology, Changzheng Hospital, Second Military Medical University, Shanghai 200003, China*

Abstract: The human pituitary tumor-transforming gene-1 (hPTTG1) has been found to be over-expressed in various cancers. Accumulated evidences implicate that some of protein kinases can specifically recognize two PXXP motifs at hPTTG1 C-terminus through their Src homology (SH3) domain and then phosphorylate the protein by their catalytic domain. Here, we integrate *in silico* analysis and *in vitro* assay to characterize the intermolecular interaction between the two hPTTG1 motif peptides [161]LGPPSPVK[168] (M1P) and [168]KMPSPPWE[175] (M2P) and the SH3 domains of Ser/Thr-specific protein kinases MAP3K and PI3K. It is identified that the two peptides bind to MAP3K SH3 domain with a moderate affinity, but cannot form stable complexes with PI3K SH3 domain. Long time scale molecular dynamics (MD) simulations reveal that the M1P peptide can fold into a standard poly-proline II helix that is bound in the peptide-binding pocket of MAP3K SH3 domain, while the M2P peptide gradually moves out of the pocket during the simulations and finally forms a weak, transient encounter complex with the domain. All these suggest that the MAP3K M1P site is a potential interacting partner of MAP3K SH3 domain, which may mediate the intermolecular recognition between hPTTG1 and MAP3K.

Key words: Human pituitary tumor-transforming gene 1 — Protein kinase — SH3 domain — Peptide — Endocrinology

Introduction

Pituitary tumor-transforming gene 1 (PTTG1) was first isolated from rat pituitary tumor cells in 1997 (Pei and Melmed 1997), and subsequently identified as a common oncogenic protein in vertebrate that is overexpressed in a variety of tumors, including those from pituitary, breast, thyroid, ovar-

ian, uterine, colon and lung (Vlotides et al. 2007). Human PTTG1 (hPTTG1) is involved in multiple cellular pathways, including proliferation, DNA repair, transformation, angiogenesis induction, invasion and the induction of genetic instability, which affects tumor invasiveness and recurrence in several systems, functions as a securin during cell cycle progression, and inhibits premature sister chromatid separation (Salehi et al. 2008). In recent years, the hPTTG1 has been established as a promising prognostic marker and new therapeutic target for pituitary adenomas, specifically in hormone-secreting tumors, in which invasiveness correlates with high levels of expression (Zhang et al. 1999a; Tfelt-Hansen et al. 2006).

Chromatin immunoprecipitation-on-chip study revealed that hPTTG1 is a global transcription factor, which exerts its transcriptional activity by either directly binding to DNA or indirectly mediating various proteins such as PTTG1IP,

* These authors contributed equally to this work.
Correspondence to: Jianmin Liu, Department of Neurosurgery, Changhai Hospital, Second Military Medical University, Shanghai 200433, China
E-mail: liu118@vip.163.com

Zhijian Yue, Department of Neurosurgery, Changhai Hospital, Second Military Medical University, Shanghai 200433, China
E-mail: yuezj638@163.com

PTTG1 binding factor, separase, p53, Sp1, MEK1, upstream stimulatory factor 1 and diverse shock proteins (Tong and Eigler 2009). In order to uncover the structural basis of hPTTG1 capable of interacting with so many biomolecular partners, Sánchez-Puig and co-workers employed biophysical characterizations to show that hPTTG1 is totally unstructured in solution and thus belongs to the family of natively unfolded proteins, which is devoid of tertiary and secondary structure except for a small amount of polyproline II (PPII) helix at its C-terminal region (Boelaert et al. 2004; Sánchez-Puig et al. 2005). Under physiological condition, the intermolecular interaction events of hPTTG1 with its diverse binding partners are regulated by a complicated combination of phosphorylation and dephosphorylation events at a variety of phosphorylatable sites (Tong and Eigler 2009). The intact hPTTG1 protein is composed of 202 amino acids, in which more than 30 residues are serine, threonine and tyrosine, implying that the protein is a primary target of protein kinases. For example, rat PTTG1 has a consensus phosphorylation site X(S/T)P within the transactivation domain and is phosphorylated by Ser/Thr-specific protein kinase at Ser162 *in vitro*, which is critical for rat PTTG1 transactivation function (Pei 2000).

A proline-rich region in hPTTG1 C-terminus contains two PXXP motifs that are potential binding targets of protein kinases having a Src homology 3 (SH3) domain (Boelaert et al. 2004). Mutation or deletion of the hPTTG1 SH3-binding motifs totally abolished transforming activity and transactivating ability of the protein, suggesting that the motifs are required for hPTTG1 functions including transformation, bFGF induction and angiogenesis (Domínguez et al. 1998; Zhang et al. 1999b). Served as a multifunctional regulator, the hPTTG1 has been found to interact with various proteins and to participate in a variety of cell signaling pathways (Tong and Eigler 2009). A number of protein kinases are involved in these pathways, which regulate hPTTG1 functions by phosphorylating the protein and its interacting factors. Protein kinases can specifically recognize and phosphorylate hPTTG1 through three approaches: (i) Low-efficiency approach: the

kinase directly catches the substrate by itself; (ii) Medium-efficiency approach: the kinase interacts with the substrate *via* a scaffolding protein which can bind the kinase and the substrate simultaneously; (iii) High-efficiency approach: the kinase recognizes the substrate using a regulatory module such as the SH3 domain. In this study, we only considered the third approach. Many kinases such as Src and Abl contain a non-catalytic SH3 domain that functions as regulatory module to determine kinase's substrate specificity by selectively targeting PXXP motif present in the substrate proteins. Previously, cell-based assays revealed that the hPTTG1 signaling pathway is essentially regulated by SH3-containing kinases MAP3K and PI3K (Pei 2000; Vlotides et al. 2006; Chen et al. 2013; Li et al. 2013). Thus, we assume that the two kinases may specifically recognize hPTTG1 SH3-binding motifs *via* their SH3 domain and then phosphorylates the hPTTG1 by their catalytic domain. In order to test the notion, we herein propose a synthetic strategy that integrates *in silico* analysis and *in vitro* assay to systematically characterize the intermolecular interaction between hPTTG1 SH3-binding motifs and the SH3 domain of MAP3K and PI3K. Based on the knowledge harvested from the analysis we also design two peptide mutants that may have potent capability to competitively disrupt the hPTTG1-kinase interaction. This work would help to elucidate the molecular mechanism and biological implication underlying hPTTG1 recognition and phosphorylation by protein kinases and to establish a synthetic protocol for the biological function inference and rational drug design of multifunctional proteins in tumor signaling networks.

Materials and Methods

Modeling complex structures of MAP3K and PI3K SH3 domains with hPTTG1 SH3-binding motifs

The hPTTG1 has two SH3-binding motifs ^{163}PPSP^{166} and ^{170}PSPP^{173} present in its C-terminal region (UniProt:
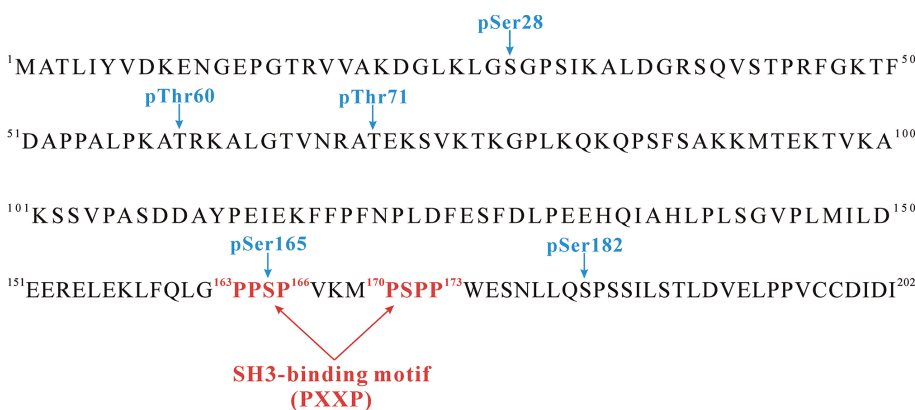
Figure 1. The hPTTG1 sequence (UniProt: O95997) as well as two SH3-binding motifs and five known phosphorylation sites in the sequence.

O95997) (Unipro 2010). Here, the sequence information of hPTTG1 as well as the two SH3-binding motifs and five known phosphorylation sites (pSer28, pThr60, pThr71, pSer165 and pSer182) in the sequence are shown in Figure 1. Considering that the residues flanking to the motifs can also contribute to SH3-ligand binding affinity and specificity, each side of a motif was extended with two additional residues to define an 8-mer sequence as the potential binding site of SH3 domain. Consequently, two extended octapeptides [161]LGPPSPVK[168] (M1P) and [168]KMPSP-PWE[175] (M2P) separately covering the two SH3-binding motifs were derived.

The complex crystal structure of PI3K SH3 domain with a 9-mer peptide KRPLPPLPS and the crystal structure of *apo* MAP3K SH3 domain were retrieved from the PDB database (Berman et al. 2000) with accession codes 3I5R and 2RF0, respectively. First, we modeled the complex structures of PI3K SH3 domain with M1P and M2P peptides. The procedure is as follows: (i) Removal of the most C-terminal Ser residue of the co-crystallized nonapeptide, resulting in the complex of PI3K SH3 domain with octapeptide KRPLPPLP. (ii) Virtual mutagenesis of the octapeptide to M1P and M2P peptide by using a graph theory-based SCWRL algorithm (Krivov et al. 2009), resulting in the low-quality complex structures of PI3K SH3 domain with M1P and M2P. (iii) The structures were minimized with YASARA server (Krieger et al. 2002) to eliminate bad atomic contacts, resulting in the refined complex structures of PI3K SH3 domain with M1P and M2P.

Subsequently, we modeled the complex structures of MAP3K SH3 domain with M1P and M2P. Since the crystal structure of MAP3K SH3 domain is in *apo* state that has no co-crystallized peptide ligand, we employed a computational strategy to graft the M1P and M2P peptides from the modeled PI3K SH3-peptide complexes to MAP3K SH3 domain. The strategy is as follows: (i) Superposition of MAP3K SH3 domain to PI3K SH3 domain in complex with M1P or M2P peptide, resulting in superposed PI3K SH3/peptide/MAP3K SH3 system. (ii) Removal of the PI3K SH3 domain from the superposed system, resulting in artificial MAP3K SH3-peptide complex. (iii) The artificial MAP3K SH3-peptide complex was minimized with YASARA server (Krieger et al. 2002), resulting in the refined complex structure of MAP3K SH3 domain with peptide.

Molecular dynamics simulations

Molecular dynamics (MD) methodology has been widely used to investigate protein-peptide binding phenomena, such as self-binding peptides (Yang et al. 2015, 2016). Here, each of the domain-peptide complex structures modeled above was solvated in a rectangular box full of explicit TIP3P water molecules (Jorgensen et al. 1983) extended 10 Å from the complex in *x*, *y* and *z* orientations. First,

the complex was in turn relaxed by 500 cycles of steepest descent minimization and 3000 cycles of conjugate gradient minimization. Subsequently, 100-ns MD simulations with time step of 2.0 fs were performed at a constant temperature of 300 K and a constant pressure of 1 atm. The Particle Mesh Ewald (PME) method (Darden et al. 1993) was used to calculate the full electrostatic energy of a unit cell in a macroscopic lattice of repeating images, and SHAKE method (Ryckaert et al. 1977) was employed to constrain all covalent bonds involving hydrogen atoms.

During the last 10-ns stable simulations snapshots of the domain-peptide complex were saved every 2 ps, yielding a total of 500 snapshots, which were used for binding free energy calculations. Molecular mechanics/Poisson-Boltzmann surface area (MM/PBSA) method was applied to the calculations (Homeyer and Gohlke 2012), which derived the interaction energy ΔE_{int} between the domain and peptide and the desolvation free energy ΔG_{dslv} upon the domain-peptide binding using molecular mechanics (MM) approach and implicit solvent model (PBSA), respectively. To consider the conformational flexibility of peptide ligand, the normal mode analysis (NMA) (Moritsugu et al. 2010) was employed to estimate entropy penalty $-T\Delta S$ upon the binding. Due to the high computational demand only 50 snapshots were used in the analysis (Hou et al. 2006). Frequencies of vibrational modes were computed at 300 K for the snapshots using a harmonic approximation of the energies. Consequently, the total binding free energy ΔG_{total} of peptide to domain can be obtained as:

$$\Delta G_{total} = \Delta E_{int} + \Delta G_{dslv} - T\Delta S \qquad (1)$$

Here, all dynamics simulations and energetics calculations were carried out using *amber ff03* force field (Duan et al. 2003) implemented with the AMBER11 suite of programs (Case et al. 2005).

Fluorescence spectroscopy assay

Peptides were synthesized using standard 9-fluorenyl methoxycarbonyl (Fmoc) solid phase chemistry, which were then purified by RP-HPLC C18 columns and confirmed by mass spectrometry and amino acid analysis. A standard fluorescence spectroscopy protocol modified from previous studies (Pisabarro and Serrano 1996; Schweimer et al. 2002) was used to perform peptide binding assay. Briefly, the fluorescence emission spectra of fluorescently active residues around the peptide-binding pocket of SH3 domain were used to monitor change in their environment upon peptide binding. Fluorescence was measured by a PerkinElmer LS-55 fluorescence spectrophotometer at an excitation wavelength of 298 nm (slit width 2 nm) and an emission wavelength of 345 nm (slit width 4 nm). The SH3 concentration was kept

at a constant (10 μM) in solution (10 mM KPi, pH 7.0). Changes in fluorescence were measured upon titration of peptide solution (6.5 mM). All experiments were performed at 25°C. Peptide affinity K_d was obtained by fitting experimental data to the equation:

$$F = [F_0 + F_\infty([pep]/K_d)]/[1+([pep]/K_d)] \qquad (2)$$

where [pep] is the peptide concentration at each measurement point, F is the measured SH3 fluorescence intensity at the given peptide concentration, F_0 is intensity in absence of peptide, and F_∞ is the maximal fluorescence intensity of the SH3 when saturated with the peptide.

Results and Discussion

The dynamics stability and energetics analysis of domain-peptide complexes

The complex structures of MAP3K and PI3K SH3 domains with M1P and M2P peptides were computationally modeled using virtual mutagenesis and grafting strategy, resulting in four complex systems namely MAP3K SH3-M1P, MAP3K SH3-M2P, PI3K SH3-M1P and PI3K-M2P. In order to explore structural dynamics stability, the four artificial complexes were separately subjected to 100-ns MD simulations. The *rmsd* fluctuation of domain-peptide complex interface was monitored during the simulations. Here, the interfacial residues are defined as all peptide residues as well as those domain residues that are within 5 Å distance from the peptide ligand. The *rmsd* fluctuation profile is a real-time measure of the complex stability during the simulations. As can be seen in Figure 2, the two complex systems of MAP3K SH3 domain with M1P and M2P peptides exhibit a stable dynamics trajectory over the whole simulations, while a larger thermal fluctuation can be observed for the two PI3K SH3-peptide complex systems.

Here, we visually examined the two MAP3K SH3-peptide complex systems at different stages of the simulations as well

as the finally equilibrated structure after 100-ns simulations. It is shown in Figure 3A that the MAP3K SH3-M1P system can well kept in a standard SH3-peptide binding mode over the whole simulations, that is, the M1P peptide is folded into a PPII helix that can be tightly bound within the peptide-binding pocket (active pocket) of MAP3K SH3 domain. The total binding free energy ΔG_{total} of M1P peptide to MAP3K SH3 domain was predicted to –6.7 kcal/mol by MM/PBSA calculation and NMA analysis using the last 10-ns MD trajectory, indicating a favorable interaction in the domain-peptide recognition. The total binding free energy (ΔG_{total} = –5.7 kcal/mol) can be decomposed into intermolecular interaction energy (ΔE_{int} = –102.7 kcal/mol), desolvation effect (ΔG_{dslv} = 69.2 kcal/mol) and entropy penalty ($-T\Delta S$ = 27.8 kcal/mol) (Table 1). As can be seen, ΔE_{int} is very favorable for the domain-peptide binding, which, however, would be largely counteracted by the unfavorable ΔG_{dslv} and $-T\Delta S$, finally resulting in a moderately favorable ΔG_{total}. Fluorometric titration assay confirmed the calculated results (Figure 4, trace B). A micromolar affinity (K_d = 96 μM) can be obtained by titration curve fitting, suggesting a moderate interaction in MAP3K SH3–M1P recognition.

According to MD simulations, the M2P peptide cannot hold in the active pocket of MAP3K SH3 domain, although the dynamics trajectory of the complex system seems stable over the simulations (Figure 2, trace B). By visually examining the system equilibrated by MD simulations, it is found that the M2P peptide moves out of SH3 active pocket due to the simulations and finally fixes at a region nearby the pocket (Figure 3B). Binding free energy analysis revealed a modestly favorable interaction between the domain and peptide with ΔG_{total} = –2.5 kcal/mol, which can be decomposed into ΔE_{int} = –76.8 kcal/mol, ΔG_{dslv} = 53.2 kcal/mol and $-T\Delta S$ = 27.8 kcal/mol (Table 1). The system was also determined to have a weak binding potency with dissociation constant K_d = 157 μM (Figure 4, trace A), suggesting an atypical encounter adduct between MAP3K SH3 domain and M2P peptide. It is worth noting that the M2P peptide contains a fluorescently active tryptophan residue that may influence the fluorescence spectroscopy assay. In
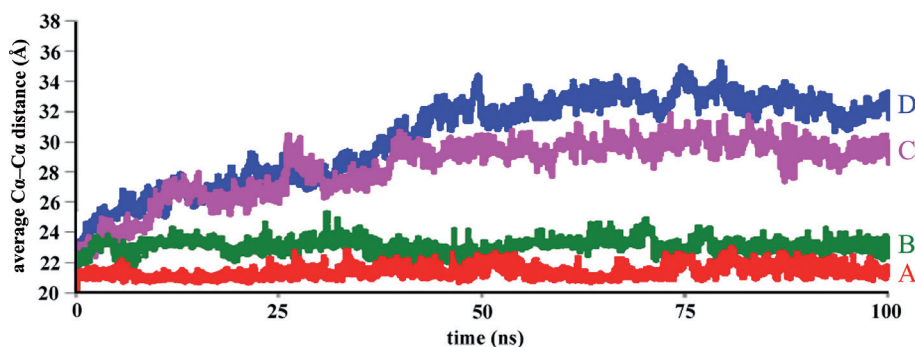
Figure 2. The *rmsd* fluctuation profiles of SH3-peptide complex interface over 100-ns MD simulations. A. MAP3K SH3-M1P system. B. MAP3K SH3-M2P system. C. PI3K SH3-M1P system. D. PI3K SH3-M2P system.
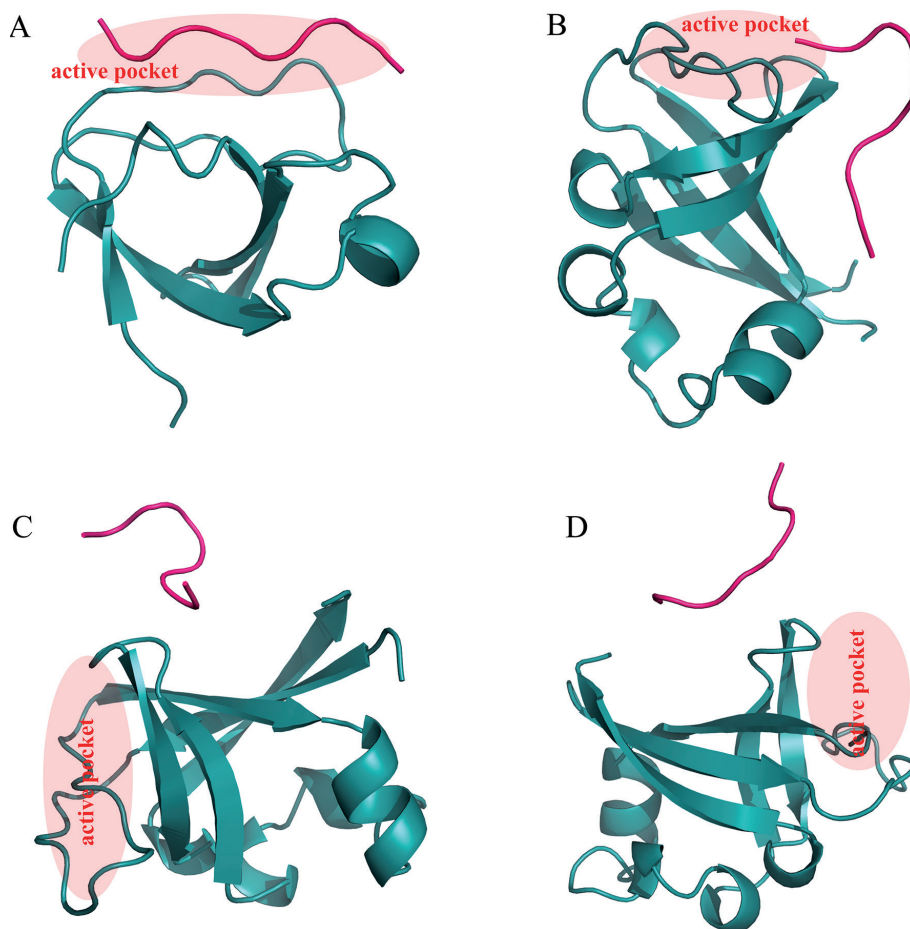
Figure 3. The equilibrated complex structures of SH3 domain and peptide ligand after 100-ns MD simulations. **A.** MAP3K SH3-M1P system. **B.** MAP3K SH3-M2P system. **C.** PI3K SH3-M1P system. **D.** PI3K SH3-M2P system. (Detailed description see in text).

particular, the fluorescence intensity increase upon titration of the peptide to SH3 solution is almost linear (Figure 4A) that may be caused by adding M2P tryptophan to the monitored solution. However, the M2P peptide has been determined to exhibit the weakest binding capability (K_d = 157 µM) to MAP3K SH3 domain in all the tested four peptides (*i.e.* M1P, M2P, M1Pm1 and M1Pm2). Therefore,

even the current binding affinity is overestimated due to the presence of M2P tryptophan residue (this means that the M2P peptide possesses a lower affinity or is a nonbinder), it would not influence our conclusion essentially.

On the other side, the peptides M1P and M2P cannot form stable complexes with PI3K SH3 domain in terms of MD simulations. As can be seen in Figure 2, trace C and D,

Table 1. The calculated energetics data and experimental affinities for peptide binding to MAP3K and PI3K SH3 domains

Domain-peptide system	Energetics (kcal/mol)				$K_d{}^e$ (µM)
	ΔE_{int}	ΔG_{dslv}	$-T\Delta S$	ΔG_{total}	
MAP3K SH3-M1P	−102.7 ± 6.2	69.2 ± 4.3	27.8 ± 6.4	−5.7 ± 0.9	96 ± 7
MAP3K SH3-M2P	−76.8 ± 3.8	53.2 ± 4.7	21.1 ± 4.8	−2.5 ± 0.4	157 ± 19
PI3K SH3-M1P	−26.4 ± 2.4	15.0 ± 1.6	9.7 ± 2.6	−1.7 ± 0.2	–
PI3K SH3-M2P	−14.8 ± 1.6	7.8 ± 0.9	6.2 ± 1.8	−0.8 ± 0.09	–
MAP3K SH3-M1Pm1	−119.3 ± 7.9	80.4 ± 5.6	30.4 ± 5.0	−8.5 ± 2.0	17 ± 1.2
MAP3K SH3-M1Pm2	−108.6 ± 5.4	71.5 ± 5.1	31.0 ± 5.7	−6.1 ± 1.5	78 ± 5

ΔE_{int}, the interaction energy between domain and peptide; ΔG_{dslv}, the desolvation free energy upon domain-peptide binding; $-T\Delta S$, the entropy penalty upon domain-peptide binding; ΔG_{total}, the total free energy of domain-peptide binding; K_d, the dissociation constant of domain-peptide binding.
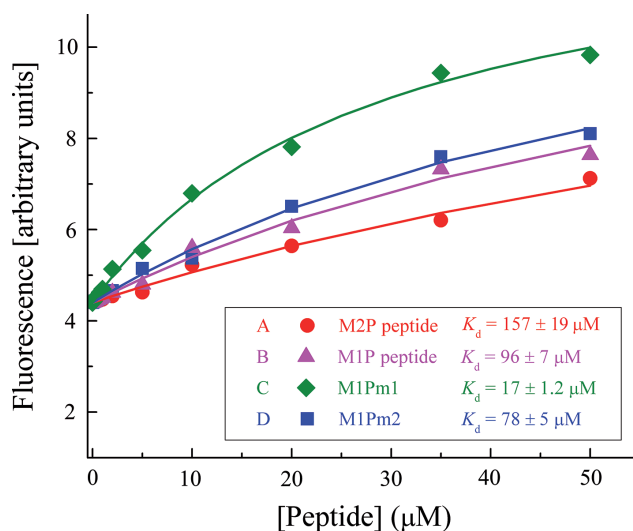
Figure 4. Titration of different peptides to the recombinant protein of MAP3K SH3 domain.

the *rmsd* changes gradually along the simulations, indicating that the two complex systems are unstable during the simulations and finally hold in an unfixed location far away from

the active pocket. In addition, the peptide ligands cannot be structured that present in a random coiled conformation after the simulations (see Figure 3C and D). All these suggest that the PI3K SH3 domain may not be the native binding partner of M1P and M2P peptides. Binding free energy calculations can also support this notion, with resulting $\Delta G_{total} = -1.7$ and -0.8 kcal/mol for the two peptides, respectively (Table 1).

Rational design of potent peptide ligands to target MAP3K SH3 domain

By combining *in silico* analysis and *in vitro* assay we demonstrated that the two hPTTG1 SH3-binding motifs have a moderate/modest affinity to MAP3K SH3 domain, suggesting that the Ser/Thr-specific protein kinase MAP3K can potentially phosphorylates hPTTG1 by recognizing and binding the motifs through its SH3 domain. MAP3K belongs to the family of mitogen-activated protein kinases (MAPKs); the kinase family is a key regulator of hPTTG1 signaling (Pei 2000; Vlotides et al. 2006; Chen et al. 2013) and has been showed to *in vitro* phosphorylate PTTG1 (Pei 2000). In the current study, it is found that the motif 1 peptide M1P of hPTTG1 can bind MAP3K SH3 domain in a standard mode
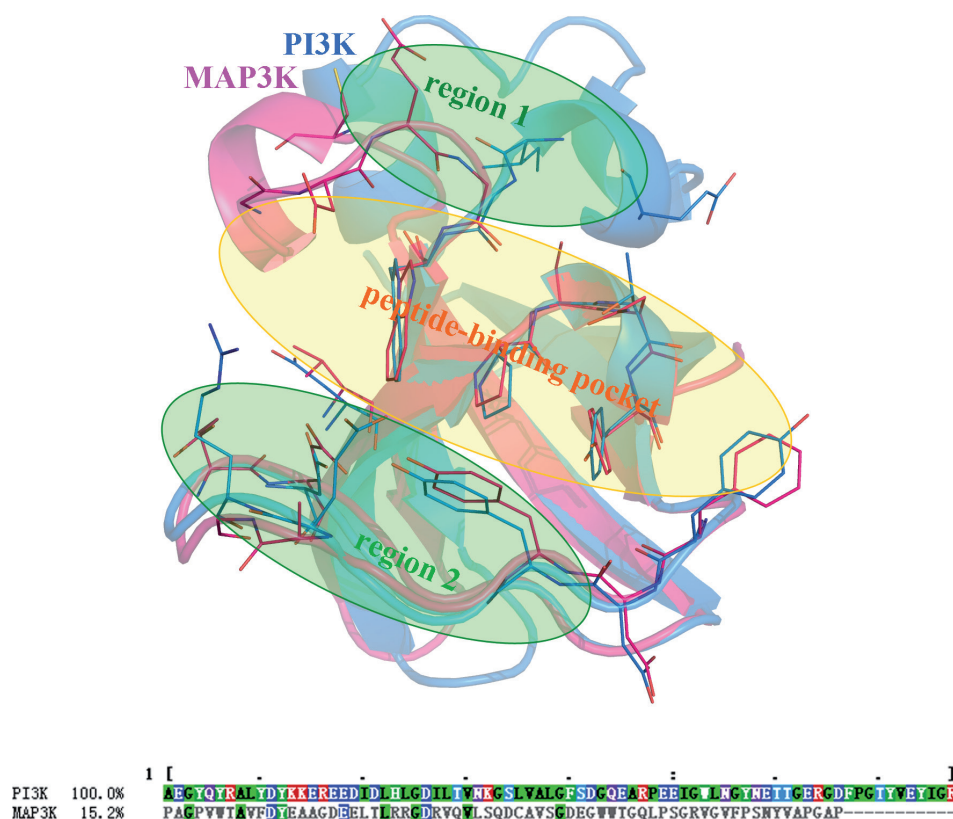
Figure 5. Sequence alignment and structural superposition between the SH3 domains of PI3K and MAP3K. (Detailed description see in text).

(PPII helix) and exhibits a potent interaction with the domain (K_d = 96 μM). Here, we attempted to modify the M1P peptide to derive mutant peptides with higher affinity for the domain. According to the modeled complex structure of MAP3K SH3 domain with M1P peptide, the positively charged Lys168 residue at peptide C-terminus can form two salt bridges with domain residues Asp26 and Glu28. A number of backbone hydrogen bonds are observed between the domain and the core region [163]PPSP[166] of the peptide, which confer stability and specificity to the complex system.

The sequence and structure similarity between the SH3 domains of MAP3K and PI3K were analyzed. As can be seen in Figure 5, the two domains have only a low sequence homology with identity = 15.2% derived from the sequence alignment using MView server (Brown et al. 1998). Structural superposition revealed that the two domains share a common folding model over global structural architecture; a conserved residue distribution pattern can be observed in their core peptide-binding pocket (Figure 5). However, there are two regions flanking to the pocket that exhibit low residue conservation over the two SH3 domains; the regions 1 and 2 are considerably and partially different between the two domains, respectively (Figure 5). Thus, the two regions may primarily contribute to peptide selectivity. By examining hydrophobic potential map on domain surface, it is evident that the peptide-binding pocket of SH3 domain can be divided into hydrophilic, hydrophobic and amphiphilic regions corresponding to the N-terminus, central part and C-terminus of peptide ligand, respectively. The central part covers peptide core motif PXXP, which defines hydrophobic interactions and backbone hydrogen bonds with the domain. Considering that this part is critical for peptide binding, we herein did not modify it. The N-terminus of peptide is very close to a negatively charged region (Asp55 and Glu56) of the domain, and we therefore considered mutating the nonpolar residue Leu161 to a positively charged residue Lys at the peptide N-terminus to match the electrostatic complementarity between domain and peptide, resulting in the M1P mutant 1 KGPPSPVK (M1Pm1). In addition, the C-terminal Lys168 residue can form two salt bridges with the domain, which was thus fixed in the modification. However, the nonpolar residue Val167 adjacent to Lys168 seems to touch on the hydrophobic patch of domain surface, of which the side chain is relative small and cannot fill in the space between the residue and domain. Thus, we considered mutating the residue to a nonpolar, bulky and flexible amino acid Leu, resulting in the M1P mutant 2 LGPPSPLK (M1Pm2).

Subsequently, the complex structures of MAP3K SH3 domain with the two mutants were computationally modeled and then subjected to 100-ns MD simulations. As might be expected, the complexes were bound tightly and the mutant peptides were always kept in PPII structure state during the simulations, suggesting a dynamics stability of the two domain-mutant complexes. The total binding free energy ΔG_{total}, as expected, were calculated to −8.5 and −6.1 kcal/mol for M1Pm1 and M1Pm2 peptides, respectively (Table 1), which are comparable to or better than that of wild-type M1P peptide (ΔG_{total} = −5.7 kcal/mol), indicating a theoretically satisfactory binding profile of the two mutants. To test the rational design, the two mutants were synthesized and their affinities to MAP3K SH3 domain were determined to K_d = 17 and 78 μM, respectively, by using fluorescence spectroscopy (Figure 4C and D), confirming a good consistence between the computational analysis and experimental assay. In particular, the affinity of M1Pm1 increases by 5.6-fold relative to that of wild-type M1P (K_d = 96 kcal/mol), which can thus be considered as a good candidate to develop peptide-like inhibitors that can competitively disrupt the native interaction between hPTTG1 and MAP3K.

Conflict of interest. The authors declare no conflict of interest.

References

Berman H. M., Westbrook J., Feng Z., Gilliland G., Bhat T. N., Weissig H., Shindyalov I. N., Bourne P. E. (2000): The protein data bank. Nucl. Acids Res. **28,** 235–242
http://dx.doi.org/10.1093/nar/28.1.235

Boelaert K., Yu R., Tannahill L. A., Stratford A. L., Khanim F. L., Eggo M. C., Moore J. S., Young L. S., Gittoes N. J., Franklyn J. A., Melmed S., McCabe C. J. (2004): PTTG's C-terminal PXXP motifs modulate critical cellular processes in vitro. J. Mol. Endocrinol. **33,** 663–677
http://dx.doi.org/10.1677/jme.1.01606

Brown N. P., Leroy C., Sander C. (1998): MView: a web-compatible database search or multiple alignment viewer. Bioinformatics **14,** 380–381
http://dx.doi.org/10.1093/bioinformatics/14.4.380

Case D. A., Cheatham T. E., Darden T., Gohlke H., Luo R., Merz K. M. Jr, Onufriev A., Simmerling C., Wang B., Woods R. J. (2005): The Amber biomolecular simulation programs. J. Comput. Chem. **26,** 1668–1688
http://dx.doi.org/10.1002/jcc.20290

Chen P. Y., Yen J. H., Kao R. H., Chen J. H. (2013): Down-regulation of the oncogene PTTG1 via the KLF6 tumor suppressor during induction of myeloid differentiation. PLoS One **8,** e71282
http://dx.doi.org/10.1371/journal.pone.0071282

Darden T., York D., Pedersen L. (1993): Particle mesh Ewald: an N-log(N) method for Ewald sums in large systems. Chem. Phys. **98,** 10089–10092
http://dx.doi.org/10.1063/1.464397

Domínguez A., Ramos-Morales F., Romero F., Rios R. M., Dreyfus F., Tortolero M., Pintor-Toro J. A. (1998): hpttg, a human homologue of rat pttg, is overexpressed in hematopoietic neoplasms.

Evidence for a transcriptional activation function of hPTTG. Oncogene **17,** 2187–2193

http://dx.doi.org/10.1038/sj.onc.1202140

Duan Y., Wu C., Chowdhury S., Lee M. C., Xiong G., Zhang W., Yang R., Cieplak P., Luo R., Lee T., Caldwell J., Wang J., Kollman P. (2003): A point-charge force field for molecular mechanics simulations of proteins based on condensed-phase quantum mechanical calculations. J. Comput. Chem. **24,** 1999–2012

http://dx.doi.org/10.1002/jcc.10349

Homeyer N., Gohlke H. (2012): Free energy calculations by the molecular mechanics Poisson-Boltzmann surface area method. Mol. Inf. **31,** 114–122

http://dx.doi.org/10.1002/minf.201100135

Hou T., Chen K., McLaughlin W. A., Lu B., Wang W. (2006): Computational analysis and prediction of the binding motif and protein interacting partners of the Abl SH3 domain. PLoS Comput. Biol. **2,** e1

http://dx.doi.org/10.1371/journal.pcbi.0020001

Jorgensen W. L., Chandrasekhar J., Madura J. D., Impey R. W., Klein M. L. (1983): Comparison of simple potential functions for simulating liquid water. J. Chem. Phys. **79,** 926–935

http://dx.doi.org/10.1063/1.445869

Krieger E., Koraimann G., Vriend G. (2002): Increasing the precision of comparative models with YASARA NOVA – a self-parameterizing force field. Proteins **47,** 393–402

http://dx.doi.org/10.1002/prot.10104

Krivov G. G., Shapovalov M. V., Dunbrack R. L. Jr. (2009): Improved prediction of protein side-chain conformations with SCWRL4. Proteins **77,** 778–795

http://dx.doi.org/10.1002/prot.22488

Li H., Yin C., Zhang B., Sun Y., Shi L., Liu N., Liang S., Lu S., Liu Y., Zhang J., Li F., Li W., Liu F., Sun L., Qi Y. (2013): PTTG1 promotes migration and invasion of human non-small cell lung cancer cells and is modulated by miR-186. Carcinogenesis **34,** 2145–2155

http://dx.doi.org/10.1093/carcin/bgt158

Moritsugu K., Njunda B. M., Smith J. C. (2010): Theory and normal-mode analysis of change in protein vibrational dynamics on ligand binding. J. Phys. Chem. B **114,** 1479–1485

http://dx.doi.org/10.1021/jp909677p

Pei L., Melmed S. (1997): Isolation and characterization of a pituitary tumor-transforming gene (PTTG). Mol. Endocrinol. **11,** 433–441

http://dx.doi.org/10.1210/mend.11.4.9911

Pei L. (2000): Activation of mitogen-activated protein kinase cascade regulates pituitary tumor-transforming gene transactivation function. J. Biol. Chem. **275,** 31191–31198

http://dx.doi.org/10.1074/jbc.M002451200

Pisabarro M. T., Serrano L. (1996): Rational design of specific high-affinity peptide ligands for the SH3 domain. Biochemistry **35,** 10634–10640

http://dx.doi.org/10.1021/bi960203t

Ryckaert J. P., Ciccotti G., Berendsen H. J. C. (1977): Numerical integration of the Cartesian equations of motion of a system with constraints: molecular dynamics of n-alkanes. J. Comput. Phys. **23,** 327–341

http://dx.doi.org/10.1016/0021-9991(77)90098-5

Salehi F., Kovacs K., Scheithauer B. W., Lloyd R. V., Cusimano M. (2008): Pituitary tumor-transforming gene in endocrine and other neoplasms: a review and update. Endocr. Relat. Cancer **15,** 721–743

http://dx.doi.org/10.1677/ERC-08-0012

Sánchez-Puig N., Veprintsev D. B., Fersht A. R. (2005): Human full-length Securin is a natively unfolded protein. Protein Sci. **14,** 1410–1418

http://dx.doi.org/10.1110/ps.051368005

Schweimer K., Hoffmann S., Bauer F., Friedrich U., Kardinal C., Feller S. M., Biesinger B., Sticht H. (2002): Structural investigation of the binding of a herpesviral protein to the SH3 domain of tyrosine kinase Lck. Biochemistry **41,** 5120–5130

http://dx.doi.org/10.1021/bi015986j

Tfelt-Hansen J., Kanuparthi D., Chattopadhyay N. (2006): The emerging role of pituitary tumor transforming gene in tumorigenesis. Clin. Med. Res. **4,** 130–137

http://dx.doi.org/10.3121/cmr.4.2.130

Tong Y., Eigler T. (2009): Transcriptional targets for pituitary tumor-transforming gene-1. J. Mol. Endocrinol. **43,** 179–185

http://dx.doi.org/10.1677/JME-08-0176

Unipro C. (2010): Ongoing and future developments at the Universal Protein Resource. Nucleic Acids Res. **39,** D214–219

Vlotides G., Cruz-Soto M., Rubinek T., Eigler T., Auernhammer C. J., Melmed S. (2006): Mechanisms for growth factor-induced pituitary tumor transforming gene-1 expression in pituitary folliculostellate TtT/GF cells. Mol. Endocrinol. **20,** 3321–3335

http://dx.doi.org/10.1210/me.2006-0280

Vlotides G., Eigler T., Melmed S. (2007): Pituitary tumor-transforming gene: physiology and implications for tumorigenesis. Endocr. Rev. **28,** 165–186

http://dx.doi.org/10.1210/er.2006-0042

Yang C., Zhang S., He P., Wang C., Huang J., Zhou P. (2015): Self-binding peptides: folding or binding? J. Chem. Inf. Model. **55,** 329–342

http://dx.doi.org/10.1021/ci500522v

Yang C., Zhang S., Bai Z., Hou S., Wu D., Huang J., Zhou P. (2016): A two-step binding mechanism for the self-binding peptide recognition of target domains. Mol. Biosyst. **12,** 1201–1213

http://dx.doi.org/10.1039/C5MB00800J

Zhang X., Horwitz G. A., Heaney A. P., Nakashima M., Prezant T. R., Bronstein M. D., Melmed S. (1999a): Pituitary tumor transforming gene (PTTG) expression in pituitary adenomas. J. Clin. Endocrinol. Metab. **84,** 761–767

http://dx.doi.org/10.1210/jcem.84.2.5432

Zhang X., Horwitz G. A., Prezant T. R., Valentini A., Nakashima M., Bronstein M. D., Melmed S. (1999b): Structure, expression, and function of human pituitary tumor-transforming gene (PTTG). Mol. Endocrinol. **13,** 156–166

http://dx.doi.org/10.1210/mend.13.1.0225